DOI: 10.1002/cmdc.201100003

Inhibition of *Mycobacterium tuberculosis* Methionine Aminopeptidases by Bengamide Derivatives

Jing-Ping Lu,[a] Xiu-Hua Yuan,[a] Hai Yuan,[a] Wen-Long Wang,[a] Baojie Wan,[b] Scott G. Franzblau,[b] and Qi-Zhuang Ye*[a]

Methionine aminopeptidase (MetAP) carries out an essential function of protein N-terminal processing in many bacteria and is a promising target for the development of novel antitubercular agents. Natural bengamides potently inhibit the proliferation of mammalian cells by targeting MetAP enzymes, and the X-ray crystal structure of human type 2 MetAP in complex with a bengamide derivative reveals the key interactions at the active site. By preserving the interactions with the conserved residues inside the binding pocket while exploring the differences between bacterial and human MetAPs around the binding pocket, seven bengamide derivatives were synthesized and evaluated for inhibition of *Mt*MetAP1a and *Mt*MetAP1c in different metalloforms, inhibition of *M. tuberculosis* growth in replicating and non-replicating states, and inhibition of human K562 cell growth. Potent inhibition of *Mt*MetAP1a and *Mt*MetAP1c and modest growth inhibition of *M. tuberculosis* were observed for some of these derivatives. Crystal structures of *Mt*MetAP1c in complex with two of the derivatives provided valuable structural information for improvement of these inhibitors for potency and selectivity.

Introduction

Methionine aminopeptidase (MetAP) is present in every cell and carries out co-translational modification by removing the N-terminal methionine residue from many nascent proteins.[1] MetAP is divided into two subtypes, namely types 1 and 2. Eukaryotic cells have both subtypes, and prokaryotic cells have only one. Deletion of either of the two MetAP genes in *Saccharomyces cerevisiae* rendered a slow growth phenotype, and lethality was observed if both genes were deleted.[2] Human type 1 and type 2 MetAPs play important roles in cell proliferation as well. For example, bengamides, a class of natural products that were isolated from marine sponge,[3] show nanomolar potency against cancer cell lines (compounds **1** and **2** in Figure 1),[4,5] and by a proteomics approach, human MetAPs were identified as the cellular targets.[6] Bengamides arrest cells at the G_1 and G_2M phases of the cell cycle,[4,7] and inhibition of MetAPs led to regulation of c-Src non-receptor tyrosine kinase activity.[8] An anticancer clinical trial was carried out with a synthetic bengamide derivative, LAF389 (**3**).[9]

In contrast to eukaryotic cells, most bacteria have a single MetAP gene, which codes for a type 1 MetAP. Deletion of this gene is lethal in *Escherichia coli*[10] and *Salmonella typhimurium*,[11] suggesting that MetAP is an essential enzyme and a promising target for the development of broad-spectrum antibiotics.[12] We recently demonstrated that a few MetAP inhibitors display significant antibacterial activity toward *E. coli* and *Bacillus subtilis* through MetAP inhibition.[13] Multiple MetAPs are not common in bacteria, but with more genomic sequences reported, two or more putative MetAP genes have been identified in a small number of bacteria. So far, 20 genomes of mycobacteria have been sequenced, and putative MetAP proteins in each mycobacterial genome, ranging from two to four, have been identified by sequence analysis. For example, *Mycobacterium tuberculosis* has two MetAP genes (*mapA* and *mapB* in the H_{37}Rv genome and *map_1* and *map_2* in the CDC1551 genome), both of which belong to type 1 MetAPs with high homology to *E. coli* MetAP.

Little is known about the biochemical properties of these putative MetAPs beyond their sequences. The protein from the *mapB* gene of *M. tuberculosis*, named *Mt*MetAP1c, was purified, and its structures in both the apo-form and in complex with methionine were reported.[14] Structural analysis revealed an SH3 binding motif in its N terminus, and potential ribosome interaction through this motif was proposed to facilitate co-translational methionine excision.[14] We recently further characterized this enzyme for metal activation and inhibition, and described three X-ray crystal structures of *Mt*MetAP1c with different inhibitors bound.[15] Interestingly, the other MetAP (from the *mapA* gene) of *M. tuberculosis*, named *Mt*MetAP1a, is shorter at the N terminus and has no such SH3 binding motif. When purified, *Mt*MetAP1a could be activated by divalent metal ions and inhibited by small molecules.[16] The mRNA transcripts of both *Mt*MetAP1a and *Mt*MetAP1c have been analyzed, and they show different levels in log phase and stationary phase, leading to the conclusion that the two MetAPs may perform

[a] *Dr. J.-P. Lu, Dr. X.-H. Yuan, Dr. H. Yuan, Dr. W.-L. Wang, Prof. Q.-Z. Ye*
Department of Biochemistry and Molecular Biology
Indiana University School of Medicine
635 Barnhill Drive, Indianapolis, IN, 46202 (USA)
Fax: (+1) 317-274-4686
E-mail: yeq@iupui.edu

[b] *B. Wan, Prof. S. G. Franzblau*
Institute for Tuberculosis Research
College of Pharmacy, University of Illinois at Chicago
Chicago, IL, 60612 (USA)

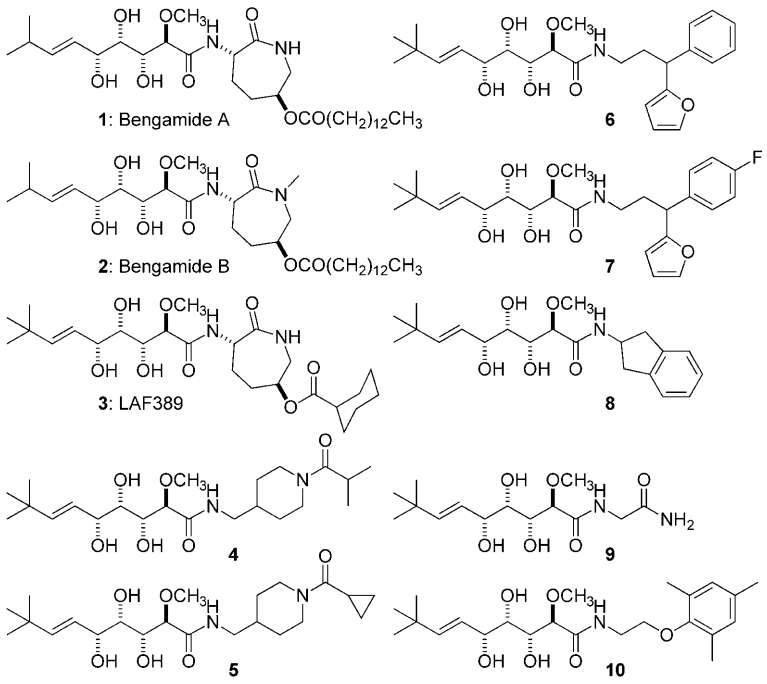

Figure 1. Chemical structures of natural bengamides **1** and **2** and their synthetic derivative **3**. Compounds **4**–**10** are the newly designed and synthesized bengamide derivatives.

important functions during different growth phases of *M. tuberculosis*.[17] The *Mt*MetAP1a gene is expressed more in log phase, whereas the *Mt*MetAP1c gene shows higher levels in the stationary phase. The high level of *Mt*MetAP1a in log phase is consistent with the recent studies demonstrating that knockdown of the *Mt*MetAP1a gene by antisense RNAs results in decreased viability of *M. tuberculosis*, whereas knockdown of the *Mt*MetAP1c gene shows little effect on growth.[18] Although *Mt*MetAP1c may not play a major role during growth phase, its high level in the stationary phase suggests its potential role during dormancy. Based on a comparison of mycobacterial genomes, it was predicted that both *Mt*MetAP1a and *Mt*MetAP1c are essential for *M. tuberculosis* survival in vivo and pathogenicity.[19] *M. tuberculosis* is unique from most prokaryotes in that it must evade and propagate within human macrophages. Therefore, the question is whether *Mt*MetAP1c plays a role in the survival of *M. tuberculosis* within mammalian cells.[18] The special characteristics of the mycobacterial life cycle may require more than one MetAP to carry out important co-translational modifications.

Tuberculosis (TB) is a deadly disease caused by mycobacterial infection, and *M. tuberculosis* is the major TB pathogen in humans. Cases of multidrug-resistant and extensively drug-resistant TB are currently happening at an alarming rate.[20] To overcome such drug resistance, new antibiotics with new mechanisms of action are urgently required. MetAP is a promising target for the development of novel drugs against TB-causing drug-resistant bacteria.[12] Herein we report several newly designed MetAP inhibitors based on natural bengamides which not only inhibit purified tubercular MetAP enzymes, but also show initial antitubercular activity. Additionally, X-ray crystal structures of *Mt*MetAP1c in complex with two such inhibitors reveal the binding mode of these bengamide derivatives and provide the structural basis for further improvement of MetAP inhibitors.

Chemistry

Design of bengamide derivatives

MetAP is a metal-dependent enzyme and requires a divalent metal ion for catalysis such as Co^{II}, Mn^{II}, Ni^{II}, or Fe^{II}.[21,22] The active site is a shallow and mostly hydrophobic pocket that accommodates the terminal methionine residue with two metal ions sitting at the bottom, as revealed in several X-ray structures.[23] Bengamides are inhibitors of both human type 1 and type 2 MetAPs with micromolar potency,[8] and their bound conformation at the active site was illustrated by the only reported X-ray structure of the bengamide derivative LAF153 (**11**) in complex with human type 2 MetAP (Figure 2A and Figure 3A, PDB code 1QZY).[6] In the dimetalated structure, the triol moiety of **11** coordinates with two Co^{II} ions to form two tetrahedral coordination geometries, reminiscent of the binding of transition-state inhibitors such as methionine phosphonate (**13**, Figure 2B, PDB code 1C23)[24] and the bestatin analogue (**14**, PDB code 3MAT).[25] It is possible that the spatial arrangement of three hydroxy groups in **11** uniquely satisfies the coordination requirement and confers high-affinity binding. On one side of the triol moiety, the *tert*-butylalkene substituent occupies the site reserved for the terminal methionine, and on the other side, the caprolactam ring beyond the amide bond interacts with residues toward the opening of the active site pocket (Figure 3A).

Most residues in the active site pockets of MetAPs of both prokaryotic and eukaryotic origin are conserved, making the interactions of an inhibitor with the residues and with the metal ions more predictable. However, variation around the opening of the pocket is significant because of the various lengths and residues in the N-terminal extension of human and bacterial MetAPs.[23] The caprolactam moiety of bengamides was believed to be essential for their potency at human MetAPs, and synthetic efforts in anticancer therapy have been directed toward modification of this moiety by introducing different functional groups on the ring while maintaining this seven-membered ring structure.[4,5,26] Our goal is the design of bengamide derivatives that show strong inhibition of tubercular MetAPs and weak or no inhibition of human MetAPs. Therefore, we kept the triol moiety and the *tert*-butylalkene substitu-

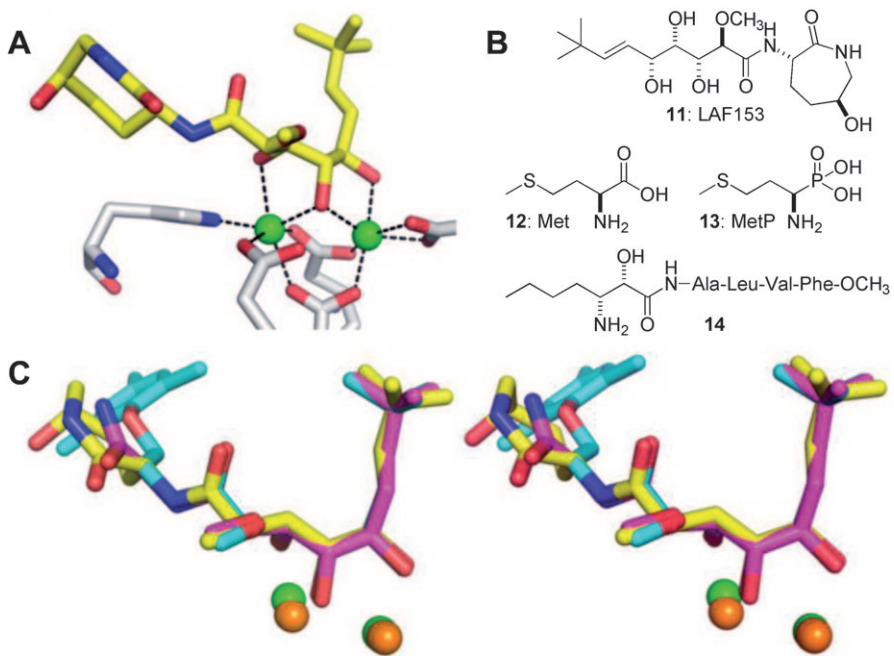

Figure 2. Design of antitubercular bengamides. A) Coordination of **11** with two metal ions inside the active site pocket of human type 2 MetAP. Color scheme: carbon, yellow (inhibitor) or grey (protein); oxygen, red; nitrogen, blue. Two Co^{II} ions are shown as green spheres. Coordination between the metal ions and the heteroatoms of the inhibitor or protein residues is shown as dashed lines. B) Chemical structures of **11**, methionine (**12**), methionine phosphonate (MetP, **13**), and the bestatin analogue **14**. C) Stereo view of the binding of newly synthesized **9** (carbon, magenta) and **10** (carbon, cyan) at the active site, in comparison with **11** (carbon, yellow); Co^{II} (green) and Mn^{II} (orange) ions are shown as spheres.

ent as the bengamide core structure for interaction with the two metal ions and with the hydrophobic methionine binding pocket. At the same time, we removed the caprolactam moiety and replaced it with various amide moieties attached to the core structure to explore the additional interactions near the opening of the active site pocket. Initially, seven such derivatives (**4**–**10**, Figure 1) were designed, synthesized, and evaluated as potential antitubercular agents.

Synthesis of bengamide derivatives

Commercially available **15** was converted into the common intermediate **16** in several steps according to a reported synthetic procedure, with minor modifications (Scheme 1).[27] Coupling of lactone **16** with various amines was accomplished by holding at reflux in isopropanol. Final deprotection produced the target compounds **4**–**10** via intermediate **17** in yields ranging from 9 to 25% for the two steps.

Results and Discussion

Inhibition of *Mt*MetAP1a and *Mt*MetAP1c

Both *Mt*MetAP1a and *Mt*MetAP1c belong to type 1 MetAPs and share high sequence homology.[16] When purified as apo-enzymes, both can be activated by divalent metal ions including Co^{II}, Mn^{II}, Ni^{II}, and Fe^{II}.[15,16] Because inhibitors of a metalloenzyme often interact directly with the metal ions at the active site, inhibitors can display marked variation in inhibitory potency toward different metalloforms of the enzyme, as we have shown for *E. coli* MetAP.[28] For therapeutic application, it is critical that these compounds can effectively inhibit the cellular enzyme in its native metalloform. We have shown that *E. coli* MetAP uses Fe^{II} for catalysis in *E. coli* cells, and inhibitors of *E. coli* MetAP with selectivity for the Fe^{II} form display antibacterial activity.[29] We

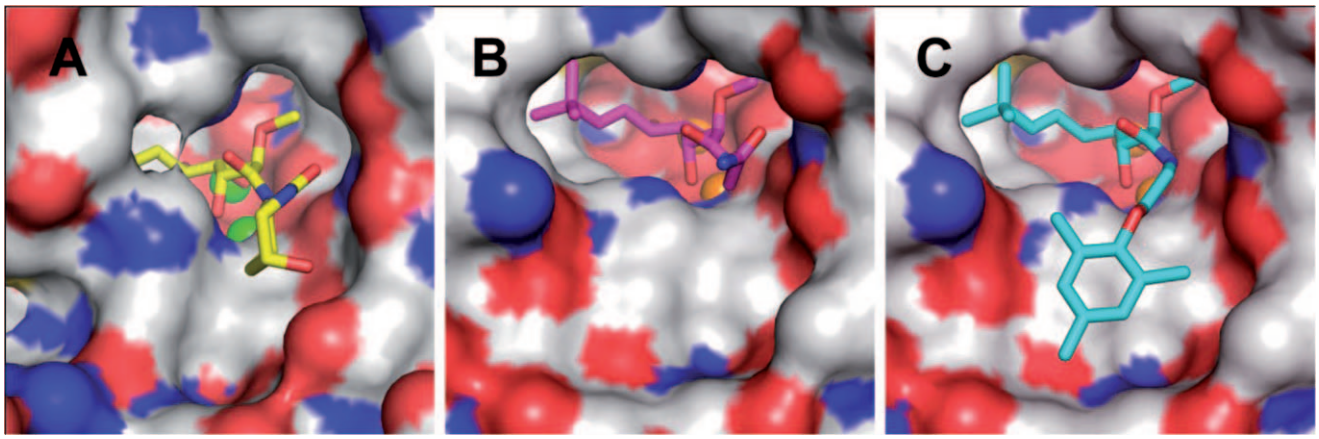

Figure 3. Binding of bengamide derivatives at the active site pocket of human type 2 MetAP and *Mt*MetAP1c. A) Inhibitor **11** (carbon, yellow) with human type 2 MetAP. B) Inhibitor **9** (carbon, magenta) with *Mt*MetAP1c. C) Inhibitor **10** (carbon, cyan) with *Mt*MetAP1c. Co^{II} (green) and Mn^{II} (orange) ions are shown as spheres. Color Scheme for enzyme surface: carbon, grey; oxygen, red; and nitrogen, blue.

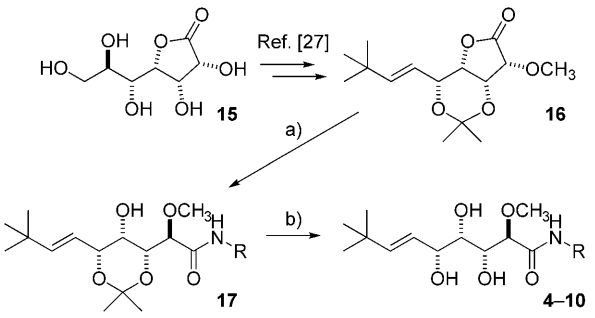

Scheme 1. Synthesis of target compounds **4**–**10** via intermediate **17**: a) *i*PrOH, R-NH_2, reflux, 10 h; b) CH_3OH, 1 N HCl, RT, 4 h. Yield range: 9–25% over two steps.

demonstrated that *Mt*MetAP1c uses Fe^{II} in *E. coli* cells,[15] but the native metalloform for *Mt*MetAP1a and *Mt*MetAP1c in *M. tuberculosis* remains unknown. Therefore, we tested the bengamide derivatives for their inhibitory activity toward *Mt*MetAP1a and *Mt*MetAP1c activated by each of the four metal ions (Table 1).

Table 1. Inhibition of MetAPs in different metalloforms and growth inhibition of *M. tuberculosis* and human K562 cells.

Compd	IC_{50} [μM]								*M. tub.* MIC [μM][a]		K562 IC_{50} [μM]
	*Mt*MetAP1a				*Mt*MetAP1c				MABA[b]	LORA[c]	
	Co	Mn	Ni	Fe	Co	Mn	Ni	Fe			
4	45	68	141	67	>250	1.3	>250	179	0%	0%	>333
5	88	187	>250	110	>250	0.96	>250	>250	0%	0%	>333
6	6.0	11	26	5.5	39	0.40	150	61	15%	8%	79.6
7	8.1	12	80	6.7	52	0.20	>250	68	48%	12%	96.5
8	31	11	140	18	>250	0.76	>250	201	29%	28%	>333
9	21	49	114	14	50	0.62	120	3.7	122	0%	>333
10	7.9	6.9	33	4.5	75	0.54	>250	42	53.9	106	37.8

[a] Minimum inhibitory concentration or percent inhibition at 128 μM. [b] Microplate Alamar Blue assay. [c] Low oxygen recovery assay. All values in this table are averages of at least triplicate determinations.

All seven derivatives **4**–**10** showed micromolar or sub-micromolar potency at the Mn^{II} form of *Mt*MetAP1c. Considering that the IC_{50} values are close to the concentration of *Mt*MetAP1c used (0.5 μM), which was limited by assay sensitivity, the actual potency for some of them could be higher. All compounds showed almost no activity against the Ni^{II} form of *Mt*MetAP1c, and their potency at the Co^{II} or Fe^{II} forms was also weak, with compounds **6**, **7**, **9**, and **10** showing relatively higher potency. Although these synthetic bengamides are clearly selective for the Mn^{II} form of *Mt*MetAP1c, the metalloform selectivity for *Mt*MetAP1a was not as noticeable. The inhibition of the Ni^{II} form of *Mt*MetAP1a was also weaker for all of the bengamides, but **6**, **7**, and **10** all showed considerable potency toward the Co^{II}, Mn^{II}, and Fe^{II} forms of *Mt*MetAP1a. Compounds **6**, **7**, **8**, and **10** all have aromatic rings in their amide moiety; it is possible that these substituents can be accommodated at the active site, and that they provide additional binding interactions.

Inhibitors of *Mt*MetAP1a and *Mt*MetAP1c were reported only recently.[15,16,18] Some of these bengamide derivatives with micromolar potency are promising lead compounds with a new scaffold for further structural modifications. It is not known which metal(s) *Mt*MetAP1a and *Mt*MetAP1c use as their native metal ion. Characterization of the metalloform-selective inhibition of these bengamides and discovery of metalloform-selective inhibitors will provide the necessary research tools to reveal the metal requirement for catalysis of MetAP in *M. tuberculosis* cells. Clearly, therapeutic MetAP inhibitors need to effectively block the function of cellular MetAPs with their native metal in place.

X-ray structures of *Mt*MetAP1c in complex with 9 and 10

The previous structure of human type 2 MetAP revealed the binding mode of **11**.[6] To confirm that the newly synthesized bengamide derivatives bind to tubercular MetAPs in the same way as designed, we obtained two X-ray crystal structures of *Mt*MetAP1c in complex with either **9** or **10** at high resolution (both at 1.25 Å, Figure 2C and Figure 3B and C). The overall fold of the new *Mt*MetAP1c structures was the same as our previously obtained structures of the same enzyme in complex with other inhibitors,[15] and two Mn^{II} ions and the new bengamide inhibitors bound at the active site pocket. Similar to **11**, both the bengamides **9** and **10** used their triol moieties to coordinate with the two active site metal ions, and the *tert*-butylalkene chain to occupy the hydrophobic S1 site.

Our strategy in designing the bengamide derivatives for selectivity was to substitute the caprolactam ring in **11** with various amide moieties to explore different interactions at the opening of the active site pocket. Indeed, the significant difference in binding was observed at the amide moiety. While the amide moiety in **9** is shorter and takes a position similar to that of the caprolactam ring in **11** (Figure 3B), the trimethylphenyl group in **10** makes a sharp turn, reaches the shallow cavity at the opening unique to *Mt*MetAP1c, and fits snugly in the cavity (Figure 3C). With this structural information on binding, additional substitutions on the phenyl ring could be introduced to explore the interactions with different residues in the cavity in order to improve both potency and selectivity.

Growth inhibition of *M. tuberculosis* at replicating state and non-replicating state

All seven newly synthesized bengamide derivatives were evaluated for their antitubercular activity against *M. tuberculosis* strain $H_{37}Rv$ (replicating phenotype, R-TB) by using a micro-

plate Alamar Blue assay,[30,31] and against *M. tuberculosis* strain H_{37}Rv-CA-lux AB (non-replicating persistent phenotype, NRP-TB) by using a low oxygen recovery assay.[32] Among the compounds tested (Table 1), compound **10** exhibited the best antitubercular activity against both replicating *M. tuberculosis* (MIC = 50.6 μM; 0.08 μM for rifampin and 0.24 μM for isoniazid) and non-replicating *M. tuberculosis* (MIC = 107.4 μM; 1.96 μM for rifampin and > 128 μM for isoniazid). Notably, **10** was also one of the best inhibitors of *Mt*MetAP1a and *Mt*MetAP1c. It is interesting that the bengamides that displayed antitubercular activity in the microplate Alamar Blue assay also displayed activity in the low oxygen recovery assay (Table 1), possibly due to inhibition of both *Mt*MetAP1a and *Mt*MetAP1c by these bengamides in cells.

Growth inhibition of human K562 cells

In the development of antitubercular bengamide derivatives, we want to minimize inhibition of human MetAPs to decrease potential toxicity. To evaluate the antiproliferative effect of these derivatives, we tested their effect on the growth of human K562 (leukemia-derived) cells (Table 1). Inhibitors **4**, **5**, **8**, and **9** showed no or weak activity at 333 μM, the highest concentration tested, and inhibitors **6**, **7**, and **10** showed low and reproducible activity. Interestingly, **10** was the best growth inhibitor of *M. tuberculosis*, and it was also the most active against the growth of human cells. Although the initial results from the limited number of bengamide derivatives are encouraging, significant improvement on potency and selectivity is required.

Conclusions

Natural bengamides with demonstrated antiproliferative potency on mammalian cells provide a unique scaffold to develop a new class of MetAP inhibitors for antibacterial and antitubercular therapeutics. Based on analysis of the binding mode of a bengamide derivative **11** on human type 2 MetAP, we replaced the caprolactam moiety in natural bengamides with various amide moieties to take advantage of differences at the inhibitor binding pocket, aiming to obtain inhibitors with high potency toward *M. tuberculosis* MetAPs and little or no potency toward human MetAPs. Some of these newly designed and synthesized bengamide derivatives showed modest but reproducible activity against both replicating and non-replicating *M. tuberculosis*. Evaluation of these derivatives on human K562 cells revealed their ability to inhibit growth, indicating their activity at mammalian MetAPs has not been completely eliminated. Importantly, the crystal structures of two such inhibitors (compounds **9** and **10**) in complex with *Mt*MetAP1c have provided valuable structural information regarding the interaction of these inhibitors with the active site and will guide the development of other bengamide derivatives with better potency and selectivity toward tubercular MetAPs.

Experimental Section

General Methods. All chemicals were reagent grade and were used without further purification. Solvents were of analytical grade. ^{1}H (500 MHz) and ^{13}C (125 MHz) NMR data were obtained on a Bruker Avance II 500 instrument. Chemical shifts (δ) are reported in ppm, using $\delta = 7.26$ ppm ($CDCl_3$, ^{1}H NMR) and $\delta = 77.23$ ppm ($CDCl_3$, ^{13}C NMR), or $\delta = 2.50$ ppm ([D_6]DMSO, ^{1}H NMR) and $\delta = 40.60$ ppm ([D_6]DMSO, ^{13}C NMR) as internal standards. Signals are reported as intervals in cases of multiplets. Signals were abbreviated as: s, singlet; d, doublet; m, multiplet. All tested compounds were at least 95% pure on the basis of HPLC–MS using an LTQ Orbitrap mass spectrometer (Thermo-Fisher Scientific) coupled to an Accela HPLC system (Thermo-Fisher Scientific). High-resolution MS data were obtained on either a Thermo Finnigan MAT-95 XP or a Waters/Micromass LCT instrument. All reactions were routinely checked by thin-layer chromatography (TLC) on silica gel 60 F_{254} (Merck) and visualized with 5% ethanolic phosphomolybdic acid solution and heat. Organic solutions were dried over anhydrous $MgSO_4$, filtered, and concentrated with a Büchi rotary evaporator at reduced pressure. Yields are of purified product and were not optimized.

General procedure for the preparation of compounds 4–10. A solution of **16** (0.1 g, 0.35 mmol) and an appropriate amine (0.9 mmol) in *i*PrOH (5 mL) was stirred at reflux for 10 h. When the amine was in the form of a HCl salt, 1.4 mmol of 2-ethylhexanoate was added.[33] The solvent was removed, and the residue was dissolved in EtOAc (20 mL), washed with 10% aq. citric acid (2× 15 mL) and aq. $NaHCO_3$ (20 mL) successively. The organic layer was dried over $MgSO_4$, filtered, concentrated to give crude acetonide intermediate **17**. The intermediate **17** was dissolved in CH_3OH (3 mL); 3 N aq. HCl in CH_3OH (1 mL) was added dropwise, and the mixture was stirred at RT for 4 h. The solution was adjusted to pH 8–9 with aq. $NaHCO_3$, and the organic solvent was removed. The residue was diluted with H_2O (10 mL) and extracted with EtOAc (2×15 mL). The combined organic layers were dried over $MgSO_4$, concentrated, and purified by column chromatography (hexane/EtOAc) to give the desired product **4**–**10**.

(2*R*,3*R*,4*S*,5*R*,*E*)-3,4,5-Trihydroxy-*N*-[(1-isobutyrylpiperidin-3-yl)-methyl]-2-methoxy-8,8-dimethylnon-6-enamide (4). Yield for two steps: 9%; ^{1}H NMR ($CDCl_3$, 500 MHz): $\delta = 1.06$ (s, 9H), 1.13 (m, 6H), 1.53–1.41 (m, 2H), 1.90–1.67 (m, 4H), 2.84–2.75 (m, 2H), 3.46–3.11 (m, 3H), 3.56 (s, 3H), 3.80–3.62 (m, 3H), 3.88–3.86 (m, 1H), 4.20–4.17 (m, 1H), 5.50–5.42 (m, 1H), 5.86–5.82 (m, 1H), 7.23 ppm (s, 1H); ^{13}C NMR ($CDCl_3$, 125 MHz): $\delta = 19.49$, 25.13, 31.11, 31.29, 33.02, 35.72, 41.35, 46.37, 60.40, 72.01, 72.52, 74.55, 82.05, 82.60, 99.99, 123.34, 145.63, 172.18, 175.84 ppm; HRMS (ESI-TOF): *m/z* 451.2784 (calcd for $C_{22}H_{40}N_2O_6Na$: 451.2784).

(2*R*,3*R*,4*S*,5*R*,*E*)-*N*-{[1-(Cyclopropanecarbonyl)piperidin-3-yl]methyl}-3,4,5-trihydroxy-2-methoxy-8,8-dimethylnon-6-enamide (5). Yield for two steps: 18%; ^{1}H NMR ($CDCl_3$, 500 MHz): $\delta = 0.78$–0.77 (m, 2H), 0.97–0.95 (m, 2H), 1.06 (s, 9H), 1.57–1.33 (m, 2H), 1.87–1.74 (m, 7H), 3.47–3.26 (m, 2H), 3.51 (s, 3H), 3.87–3.78 (m, 2H), 4.30–4.16 (m, 2H), 5.48–5.40 (m, 1H), 5.86–5.85 (m, 1H), 7.29 ppm (s, 1H); ^{13}C NMR ($CDCl_3$, 125 MHz): $\delta = 7.40$, 10.92, 24.63, 28.40, 29.42, 33.03, 35.66, 41.35, 45.52, 46.16, 46.55, 60.20, 72.25, 74.66, 82.3, 99.99, 123.29, 145.68, 172.12, 172.27 ppm; HRMS (ESI-TOF): *m/z* calcd for $C_{22}H_{38}N_2O_6Na$: 449.2628; found: 449.2606.

(2*R*,3*R*,4*S*,5*R*,*E*)-*N*-[3-(Furan-2-yl)-3-phenylpropyl]-3,4,5-trihydroxy-2-methoxy-8,8-dimethylnon-6-enamide (6). Yield for two steps: 16%; ^{1}H NMR ($CDCl_3$, 500 MHz): $\delta = 1.01$ (s, 9H), 2.15–2.14 (m, 1H), 2.37–2.35 (m, 1H), 3.33–3.27 (m, 2H), 3.47 (s, 3H), 3.57–

3.52 (m, 2H), 3.69–3.67 (m, 1H), 3.78–3.77 (m, 1H), 3.99–3.98 (m, 1H), 4.21–4.20 (m, 2H), 5.44–5.39 (dd, 1H), 5.85–5.81 (d, 1H), 6.07 (s, 1H), 6.29 (s, 1H), 6.86 (s, 1H), 7.25–7.22 (m, 3H), 7.33–7.30 ppm (m, 3H); ^{13}C NMR ($CDCl_3$, 125 MHz): δ = 14.16, 29.46, 29.70, 31.62, 33.03, 34.25, 37.67, 43.17, 59.89, 72.42, 74.57, 81.13, 105.80, 110.16, 123.20, 127.03, 127.70, 128.76, 141.57, 145.91, 156.68, 172.53 ppm; HRMS (ESI-TOF): *m/z* calcd for $C_{25}H_{35}NO_6Na$: 468.2362; found: 468.2357.

(2*R*,3*R*,4*S*,5*R*,*E*)-*N*-[3-(4-Fluorophenyl)-3-(furan-2-yl)propyl]-3,4,5-trihydroxy-2-methoxy-8,8-dimethylnon-6-enamide (7). Yield for two steps: 10%; ^{1}H NMR ($CDCl_3$, 500 MHz): δ = 1.07 (s, 9H), 2.16–2.13 (m, 1H), 2.37–2.35 (m, 1H), 3.04 (s, 1H), 3.35–3.27 (m, 2H), 3.52–3.51 (d, 1.9 Hz, 3H), 3.61–3.59 (m, 1H), 3.72–3.70 (dd, 1H), 3.82–3.96 (m, 1H), 4.02–3.99 (m, 1H), 4.17–4.15 (m, 1H), 4.24–4.22 (m, 1H), 5.47–5.42 (dd, 1H), 5.88–5.84 (d, 1H), 6.10–6.09 (m, 1H), 6.33–6.32 (m, 1H), 6.90–6.80 (m, 1H), 7.04–7.01 (m, 2H), 7.24–7.23 (m, 2H), 7.35 ppm (d, 1H); ^{13}C NMR ($CDCl_3$, 125 MHz): δ = 29.42, 33.04, 34.38, 37.58, 42.38, 60.20, 72.38, 81.19, 99.99, 105.88, 110.21, 115.50, 123.18, 129.16, 141.77, 145.99, 160.83, 162.78, 172.52 ppm; HRMS (ESI-TOF): *m/z* calcd for $C_{25}H_{34}FNO_6Na$: 486.2268; found: 486.2253.

(2*R*,3*R*,4*S*,5*R*,*E*)-*N*-(2,3-Dihydro-1*H*-inden-2-yl)-3,4,5-trihydroxy-2-methoxy-8,8-dimethylnon-6-enamide (8). Yield for two steps: 25%; ^{1}H NMR ($CDCl_3$, 500 MHz): δ = 1.05 (s, 9H), 2.89–2.83 (m, 2H), 3.41–3.36 (m, 2H), 3.49 (s, 3H), 3.61–3.60 (d, 1H), 3.75–3.74 (d, 1H), 3.83–3.82 (d, 1H), 4.26–4.23 (m, 1H), 4.79–4.77 (m, 1H), 5.46–5.42 (dd, 1H), 5.88–5.84 (d, 1H), 7.08–7.07 (d, 1H), 7.24–7.21 ppm (m, 4H); ^{13}C NMR ($CDCl_3$, 125 MHz): δ = 29.42, 33.05, 40.00, 50.14, 59.79, 72.36, 72.44, 74.59, 81.19, 123.19, 124.80, 126.97, 140.40, 145.98, 172.29 ppm; HRMS (ESI-TOF): *m/z* calcd for $C_{21}H_{31}NO_5Na$: 400.2100; found: 400.2082.

(2*R*,3*R*,4*S*,5*R*,*E*)-*N*-(2-Amino-2-oxoethyl)-3,4,5-trihydroxy-2-methoxy-8,8-dimethylnon-6-enamide (9). Yield for two steps: 14%; ^{1}H NMR ($CDCl_3$, 500 MHz): δ = 1.01 (s, 9H), 3.51 (s, 2H), 3.79 (s, 3H), 3.83–3.92 (m, 2H), 4.16–4.21 (m, 1H), 4.25–4.30 (m, 1H), 5.37–5.45 (m, 1H), 5.83–6.01 ppm (m, 1H); ^{13}C NMR ($CDCl_3$, 125 MHz): δ = 29.28, 42.72, 60.00, 66.29, 73.00, 74.30, 81.80, 99.71, 121.27, 145.62, 169.25, 170.71 ppm; HRMS (ESI-TOF) *m/z* calcd for $C_{14}H_{26}N_2O_6Na$: 341.1689; found: 341.1689.

(2*R*,3*R*,4*S*,5*R*,*E*)-3,4,5-Trihydroxy-*N*-[2-(mesityloxy)ethyl]-2-methoxy-8,8-dimethylnon-6-enamide (10). Yield for two steps: 15%; ^{1}H NMR ($CDCl_3$, 500 MHz): δ = 1.06 (s, 9H), 2.22 (s, 9H), 3.59 (s, 3H), 3.63–3.88 (m, 7H), 4.25–4.28 (m, 1H), 5.44–5.48 (dd, 1H), 5.85–5.88 (d, 1H), 6.85 (s, 2H), 7.53 ppm (s, 1H); ^{13}C NMR ($CDCl_3$, 125 MHz): δ = 16.15, 20.65, 29.44, 33.04, 39.46, 60.15, 70.10, 72.39, 72.67, 74.59, 80.89, 123.21, 129.61, 130.15, 133.66, 145.88, 152.74, 172.81 ppm; HRMS (ESI-TOF): *m/z* calcd for $C_{23}H_{37}NO_6Na$: 446.2519; found: 446.2505.

***Mt*MetAP1a and *Mt*MetAP1c inhibition assays.** *Mt*MetAP1a and *Mt*MetAP1c were expressed in *E. coli* and purified as apo-enzymes as previously described.[15,16] Both can be activated by Co^{II}, Mn^{II}, Ni^{II}, and Fe^{II} instantly. Enzymatic activity was monitored by fluorescence (λ_{ex} = 360 nm, λ_{em} = 460 nm) on a Spectramax Gemini XPS plate reader (Molecular Devices, Sunnyvale, CA, USA) following hydrolysis of the fluorogenic substrate, methionyl aminomethylcoumarin (Met-AMC), at room temperature as described.[22] All kinetics experiments were carried out on 384-well plates. For inhibition of *Mt*MetAP1a, each well contained 80 μL assay mixture with 50 mM MOPS (pH 7.5), 100 μM Met-AMC, apo-enzyme and metal ions (50 nM enzyme, 50 μM $CoCl_2$; 200 nM enzyme, 250 μM $MnCl_2$; 12.5 nM enzyme, 50 μM $NiCl_2$; or 50 nM enzyme, 10 μM $FeCl_2$, 10 μM ascorbic acid). For inhibition of *Mt*MetAP1c, each well contained 80 μL assay mixture with 50 mM MOPS (pH 7.5), 100 μM Met-AMC, apo-enzyme (500 nM), and metal ions (50 μM $CoCl_2$, 250 μM $MnCl_2$, 50 μM $NiCl_2$, or 10 μM $FeCl_2$ plus 10 μM ascorbic acid). The inhibitors were tested at six or more serially diluted concentrations. IC_{50} values were calculated from nonlinear regression curve fitting of percent inhibition values as a function of inhibitor concentration.

***M. tuberculosis* MABA and LORA assays.** Minimum inhibitory concentrations (MICs) against replicating and non-replicating cultures of *M. tuberculosis* were determined by microplate Alamar Blue assay (MABA)[30,31] and low oxygen recovery assay (LORA),[32] respectively. The former was determined against *M. tuberculosis* H_{37}Rv ATCC 27294 (American Type Culture Collection) following 7 days incubation with test samples. The latter was determined against low oxygen adapted *M. tuberculosis* H_{37}Rv lux AB carrying a luciferase reporter gene following 10 days incubation under low oxygen, followed by 28 h normoxic recovery. Both assays were conducted in microplate format in 7H12 medium.[30] MIC values are defined as the lowest concentration effecting a decrease of $\geq$0% in fluorescence (MABA) or luminescence (LORA) relative to untreated controls.

Crystallization and data collection. Crystals of the enzyme–inhibitor complexes were obtained independently by a hanging-drop vapor-diffusion method at room temperature. Each of the inhibitors (**9** or **10**; 100 mM in DMSO) was added to concentrated metalated enzyme (10 mg mL^{-1}, 0.32 mM protein; 2 mM metal) in 50 mM Tris, pH 8.0, 150 mM NaCl, and the molar ratio of inhibitor to *Mt*MetAP1c was 5:1 or 10:1. The enzyme–inhibitor mixture was mixed with a reservoir buffer at a 1:1 ratio. The reservoir buffer was 100 mM Bis-Tris (pH 5.5), 1.3 M $(NH_4)_2SO_4$, and 10% glycerol. Diffraction data were collected at the Advanced Photon Source, Argonne National Laboratory (beamlines 19ID and 19BM) and were processed with HKL3000.[34] Both crystals belong to space group $P6_3$. One molecule is in the asymmetric unit.

Structural solution and refinement. Structures were solved by molecular replacement with MolRep[35] in CCP4[36] with CCP4i interface,[37] using our previously published *Mt*MetAP1c structure (PDB code 3IU7)[15] as the search model. The structure was refined with REFMAC5[38] with iterative model building using WinCoot.[39] The refinement was monitored with 5% of the reflections set aside for R_{free} factor analysis throughout the entire refinement process. Electron density was clear for almost all residues, and residues from the second (P2) in the native protein to the end (L285) were modeled. Comparison of structures and generation of structural drawings were carried out by using PyMOL.[40] Statistical parameters in data collection and structural refinement are listed in Table 2. Atomic coordinates and structure factors for the two structures have been deposited in the RCSB Protein Data Bank.

Human K562 growth inhibition assay. K562 cells from ATCC were cultured as suspension in RPMI 1640 medium, containing 10% newborn calf serum. Growth inhibition assays were carried out in a total volume of 120 μL in each well on 96-well white plates. Compounds were serially (twofold) diluted to 12 concentrations, and cells were seeded at 12000 cells per well by dispensing suspended K562 cells in growth medium with an eight-channel automated MultiDrop liquid dispenser. The plates were incubated at 37 °C in a humidified 5% CO_2 incubator for 48 h. A modified luciferase activity assay was used to monitor cell growth. A mixture of luciferase, luciferin, Triton X-100, and $MgCl_2$ in a total volume of 80 μL was added to the cells in each well, and luminescence was determined

Table 2. X-ray crystallographic data collection and refinement statistics.

Parameter	9	10
Space group:	$P6_3$	$P6_3$
a [Å]	106.0	106.0
b [Å]	106.0	106.0
c [Å]	50.3	50.4
α [°]	90	90
β [°]	90	90
γ [°]	120	120
Data Collection		
Resolution range [Å]	50–1.25 (1.27–1.25)[a]	50–1.25 (1.27–1.25)
Collected reflections	559494	633834
Unique reflections	85942	89260
Completeness [%]	97.0 (73.9)	100 (100)
I/σ (I)	40.0 (1.7)	36.8 (3.3)
R_{merge} [%]	5.3 (47.5)	5.7 (52.5)
Refinement Statistics		
R [%]	16.8	16.9
R_{free} [%]	18.1	18.8
RMSD bonds [Å]	0.032	0.033
RMSD angles [°]	2.49	2.51
No. solvent molecules	211	223
B protein [Å^2]	13.1	12.2
B inhibitor [Å^2]	11.7	10.5
B water [Å^2]	19.4	19.0

[a] Values given in parentheses correspond to the outer shell of data.

on a Spectramax Gemini or Spectramax M5 plate reader. The IC_{50} values were calculated from nonlinear regression curve fitting of percent inhibition values as a function of inhibitor concentration.

Abbreviations: MetAP, methionine aminopeptidase; *Mt*MetAP1a, *M. tuberculosis* methionine aminopeptidase type 1a; *Mt*MetAP1c, *M. tuberculosis* methionine aminopeptidase type 1c; Met-AMC, methionyl aminomethylcoumarin; TB, tuberculosis.

PDB ID codes: Coordinates and structure factors for *Mt*MetAP1c complexed to compounds **9** and **10** have been deposited in the RCSB Protein Data Bank (PDB) under access codes 3PKB and 3PKA, respectively.

Acknowledgements

This work was supported by National Institutes of Health Research Grants R01 AI065898 and R56 AI065898, and by a Research Support Fund Grant and a Biomedical Research Grant from Indiana University (to Q.-Z.Y.). We thank the staffs at the Structural Biology Center of the Advanced Photon Source, Argonne National Laboratory (beamlines 19ID and 19BM) for assistance with X-ray diffraction data collection.

Keywords: antibiotics · drug discovery · inhibitors · hydrolases · metalloenzymes

[1] R. A. Bradshaw, W. W. Brickey, K. W. Walker, *Trends Biochem. Sci.* **1998**, *23*, 263 – 267.
[2] X. Li, Y. H. Chang, *Proc. Natl. Acad. Sci. USA* **1995**, *92*, 12357 – 12361.
[3] E. Quinoa, M. Adamczeski, P. Crews, G. J. Bakus, *J. Org. Chem.* **1986**, *51*, 4494 – 4497.
[4] F. R. Kinder, Jr., R. W. Versace, K. W. Bair, J. M. Bontempo, D. Cesarz, S. Chen, P. Crews, A. M. Czuchta, C. T. Jagoe, Y. Mou, R. Nemzek, P. E. Phillips, L. D. Tran, R. M. Wang, S. Weltchek, S. Zabludoff, *J. Med. Chem.* **2001**, *44*, 3692 – 3699.
[5] Z. Thale, F. R. Kinder, K. W. Bair, J. Bontempo, A. M. Czuchta, R. W. Versace, P. E. Phillips, M. L. Sanders, S. Wattanasin, P. Crews, *J. Org. Chem.* **2001**, *66*, 1733 – 1741.
[6] H. Towbin, K. W. Bair, J. A. DeCaprio, M. J. Eck, S. Kim, F. R. Kinder, A. Morollo, D. R. Mueller, P. Schindler, H. K. Song, J. van Oostrum, R. W. Versace, H. Voshol, J. Wood, S. Zabludoff, P. E. Phillips, *J. Biol. Chem.* **2003**, *278*, 52964 – 52971.
[7] P. E. Phillips, K. W. Bair, J. Bontempo, P. Crews, Czuchta, A. M. , F. R. Kinder, A. Vattay, R. W. Versace, B. Wang, J. Wang, A. Wood, S. Zabludoff, *Proc. Am. Assoc. Cancer Res.* **2000**, *41*, 59.
[8] X. Hu, Y. Dang, K. Tenney, P. Crews, C. W. Tsai, K. M. Sixt, P. A. Cole, J. O. Liu, *Chem. Biol.* **2007**, *14*, 764 – 774.
[9] H. Dumez, H. Gall, R. Capdeville, C. Dutreix, A. T. van Oosterom, G. Giaccone, *Anticancer Drugs* **2007**, *18*, 219 – 225.
[10] S. Y. Chang, E. C. McGary, S. Chang, *J. Bacteriol.* **1989**, *171*, 4071 – 4072.
[11] C. G. Miller, A. M. Kukral, J. L. Miller, N. R. Movva, *J. Bacteriol.* **1989**, *171*, 5215 – 5217.
[12] M. D. Vaughan, P. B. Sampson, J. F. Honek, *Curr. Med. Chem.* **2002**, *9*, 385 – 409.
[13] a) S. C. Chai, Q. Z. Ye, *Bioorg. Med. Chem. Lett.* **2010**, *20*, 2129 – 2132; b) W. L. Wang, S. C. Chai, Q. Z. Ye, *Bioorg. Med. Chem. Lett.* **2009**, *19*, 1080 – 1083; c) W. L. Wang, S. C. Chai, M. Huang, H. Z. He, T. D. Hurley, Q. Z. Ye, *J. Med. Chem.* **2008**, *51*, 6110 – 6120.
[14] A. Addlagatta, M. L. Quillin, O. Omotoso, J. O. Liu, B. W. Matthews, *Biochemistry* **2005**, *44*, 7166 – 7174.
[15] J. P. Lu, S. C. Chai, Q. Z. Ye, *J. Med. Chem.* **2010**, *53*, 1329 – 1337.
[16] J. P. Lu, Q. Z. Ye, *Bioorg. Med. Chem. Lett.* **2010**, *20*, 2776 – 2779.
[17] X. Zhang, S. Chen, Z. Hu, L. Zhang, H. Wang, *Curr. Microbiol.* **2009**, *59*, 520 – 525.
[18] O. Olaleye, T. R. Raghunand, S. Bhat, J. He, S. Tyagi, G. Lamichhane, P. Gu, J. Zhou, Y. Zhang, J. Grosset, W. R. Bishai, J. O. Liu, *Chem. Biol.* **2010**, *17*, 86 – 97.
[19] M. L. Ribeiro-Guimaraes, M. C. Pessolani, *Microb. Pathog.* **2007**, *43*, 173 – 178.
[20] A. S. Fauci, *J. Inf. Dis.* **2008**, *197*, 1493 – 1498.
[21] V. M. D'Souza, R. C. Holz, *Biochemistry* **1999**, *38*, 11079 – 11085.
[22] J. Y. Li, L. L. Chen, Y. M. Cui, Q. L. Luo, J. Li, F. J. Nan, Q. Z. Ye, *Biochem. Biophys. Res. Commun.* **2003**, *307*, 172 – 179.
[23] W. T. Lowther, B. W. Matthews, *Biochim. Biophys. Acta* **2000**, *1477*, 157 – 167.
[24] W. T. Lowther, Y. Zhang, P. B. Sampson, J. F. Honek, B. W. Matthews, *Biochemistry* **1999**, *38*, 14810 – 14819.
[25] W. T. Lowther, A. M. Orville, D. T. Madden, S. Lim, D. H. Rich, B. W. Matthews, *Biochemistry* **1999**, *38*, 7678 – 7688.
[26] a) G. Liu, Y. M. Ma, W. Y. Tai, C. M. Xie, Y. L. Li, J. Li, F. J. Nan, *ChemMedChem* **2008**, *3*, 74 – 78; b) F. R. Kinder, Jr., S. Wattanasin, R. W. Versace, K. W. Bair, J. Bontempo, M. A. Green, Y. J. Lu, H. R. Marepalli, P. E. Phillips, D. Roche, L. D. Tran, R. Wang, L. Waykole, D. D. Xu, S. Zabludoff, *J. Org. Chem.* **2001**, *66*, 2118 – 2122.
[27] D. D. Xu, L. Waykole, J. V. Calienni, L. Ciszewski, G. T. Lee, W. Liu, J. Szewczyk, K. Vargas, K. Prasad, O. Repic, T. J. Blacklock, *Org. Process Res. Dev.* **2003**, *7*, 856 – 865.
[28] Q. Z. Ye, S. X. Xie, M. Huang, W. J. Huang, J. P. Lu, Z. Q. Ma, *J. Am. Chem. Soc.* **2004**, *126*, 13940 – 13941.
[29] S. C. Chai, W. L. Wang, Q. Z. Ye, *J. Biol. Chem.* **2008**, *283*, 26879 – 26885.
[30] K. Falzari, Z. Zhu, D. Pan, H. Liu, P. Hongmanee, S. G. Franzblau, *Antimicrob. Agents Chemother.* **2005**, *49*, 1447 – 1454.
[31] L. Collins, S. G. Franzblau, *Antimicrob. Agents Chemother.* **1997**, *41*, 1004 – 1009.
[32] S. H. Cho, S. Warit, B. Wan, C. H. Hwang, G. F. Pauli, S. G. Franzblau, *Antimicrob. Agents Chemother.* **2007**, *51*, 1380 – 1385.
[33] W. Liu, D. D. Xu, O. Repic, T. J. Blacklock, *Tetrahedron Lett.* **2001**, *42*, 2439 – 2441.
[34] W. Minor, M. Cymborowski, Z. Otwinowski, M. Chruszcz, *Acta Crystallogr. Sect. D* **2006**, *62*, 859 – 866.
[35] A. Vagin, A. Teplyakov, *J. Appl. Crystallogr.* **1997**, *30*, 1022 – 1025.

[36] Collaborative Computational Project Number 4, *Acta Crystallogr.* **1994**, *D50*, 760 – 763.
[37] E. Potterton, P. Briggs, M. Turkenburg, E. Dodson, *Acta Crystallogr. D Biol. Crystallogr.* **2003**, *59*, 1131 – 1137.
[38] G. N. Murshudov, A. A. Vagin, E. J. Dodson, *Acta Crystallogr. Sect. D* **1997**, *53*, 240 – 255.
[39] P. Emsley, K. Cowtan, *Acta Crystallogr. Sect. D* **2004**, *60*, 2126 – 2132.
[40] The PyMOL Molecular Graphics System, Version 1.3, Schrödinger, LLC (**2002**): http://www.pymol.org (accessed March 14, 2011).

Received: January 7, 2011
Revised: March 1, 2011
Published online on April 4, 2011

